ACS OMEGA

Open Access

http://pubs.acs.org/journal/acsodf

Article

Oxidative and Extractive Desulfurization of Fuel Oils Catalyzed by *N*-Carboxymethyl Pyridinium Acetate and *N*-Carboxyethyl Pyridinium Acetate Acidic Ionic Liquids: Experimental and Computational DFT Study

Amani Sager, Shofiur Rahman,* Syed A. Imtiaz,* Yan Zhang,* Abdullah Alodhayb, Paris E. Georghiou,* and Mahmoud Al-Gawati

Cite This: *ACS Omega* 2024, 9, 23485−23498

Read Online

ACCESS | Metrics & More | Article Recommendations | Supporting Information

ABSTRACT: This study reports on the synthesis, characterization, and application of two acidic ionic liquids, namely, *N*-carboxymethylpyridinium acetate ($[HO_2CCH_2Py][CH_3CO_2]$ or **AIL1**) and *N*-carboxyethylpyridinium acetate ($[HO_2C(CH_2)_2Py][CH_3CO_2]$ or **AIL2**), as both extractants and catalysts for the oxidative and extractive desulfurization (OEDS) of model fuel oils containing heteroaromatic sulfur compounds. The structural properties of the synthesized acidic ionic liquids (ILs) were confirmed by ^{1}H NMR, ^{13}C NMR, and FT-IR spectroscopic analysis. To optimize the performance of the acidic AILs in the desulfurization process, the effects of different parameters, such as H_2O_2 dosage, reaction time, and temperatures, were investigated. The experimental results showed that **AIL1** has exceptionally high desulfurization−extraction rates, with values of 99.8%, 97.8%, and 95.4%, for DBT, BT, and 4,6-DMDBT, respectively, under the optimum conditions established. Under the same conditions, the desulfurization-extraction rates using **AIL2** reached 91.6%, 87.3%, and 82.4%, respectively, for DBT, 4, 6-DMDBT, and BT. Both ionic liquids can be recycled up to 9 times without a significant decrease in their sulfur removal efficiencies. Furthermore, density functional theory (DFT) calculations were conducted to evaluate the electronic interaction energies (ΔIE) between the AILs with each of the sulfur-containing compounds and their putative oxidized products. The computational findings strongly supported the experimental outcomes.

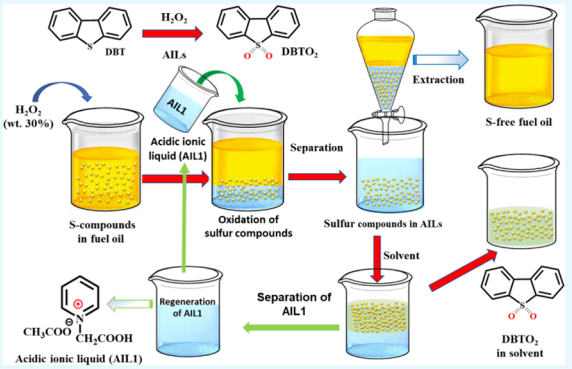

1. INTRODUCTION

In recent decades, the increasing levels of additional environmental pollution resulting from the emission of sulfur oxides (SOx) have been a major cause for concern.[1−4] These gases, which can significantly threaten public health and the environment, are released into the atmosphere from the burning of fossil fuels containing sulfur. Therefore, it is crucial to remove sulfur from fuels to protect the environment and promote sustainable development. Desulfurization therefore plays a crucial role in minimizing harmful SOx emissions, thus reducing their polluting impact on the environment.

One of the most common methods used for removing sulfur contaminants in petroleum products is hydrodesulfurization (HDS).[5−10] This process can easily remove lower molecular weight sulfur compounds, such as thiols, sulfides, and disulfides. Unfortunately, this method requires a high temperature and high pressure of hydrogen. Furthermore, this approach has several other drawbacks, including its ineffectiveness in eliminating sulfur-containing heteroaromatic compounds, such as benzothiophene (BT), dibenzothiophene (DBT), and their alkyl derivatives. The reactivities of these commonly occurring petroleum fuel sulfur compounds are found to be in the following order: BT > alkylated-BT > DBT > 4 or 6-MDBT > 4,6-DMDBT.

Beyond the conventional hydrodesulfurization method, there are a few different approaches to desulfurization, and these include adsorptive desulfurization (ADS),[11−18] extractive desulfurization (EDS),[19−23] biodesulfurization (BDS),[24,25] oxidative desulfurization (ODS),[26−32] and oxidative-extractive desulfurization (OEDS).[33−36] Adsorptive desulfurization involves the treatment of a fuel with an activated/functionalized adsorbent to remove the sulfur under mild temperature (ranging from room temperature to around 100 °C)

Received: January 17, 2024
Revised: April 3, 2024
Accepted: April 4, 2024
Published: May 21, 2024

Scheme 1. Synthesis Route for *N*-Carboxymethylpyridinium Acetate (AIL1) and *N*-Carboxyethylpyridinium Acetate (AIL2) Acidic Ionic Liquids

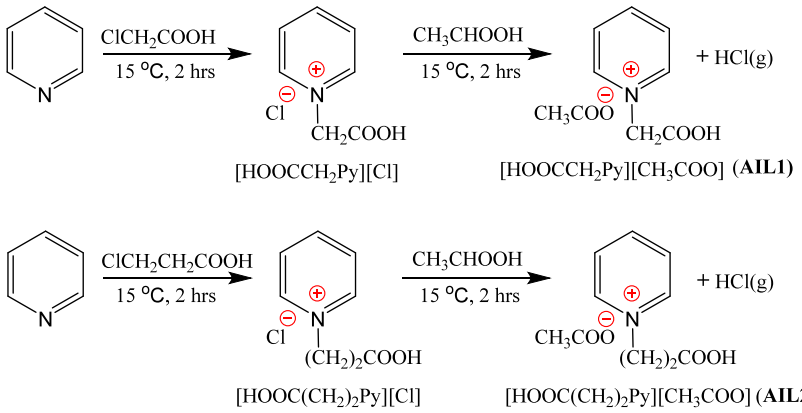

conditions. The most common adsorbents that have been reported in studies with model fuels include molecular sieves, graphene, graphene-like materials,[11] activated carbon,[12,13] metal−organic frameworks (MOFs),[14,15] and zeolites.[18] However, the preparation of solid adsorbent materials is usually complicated, and desulfurization with real fossil fuel oil has not been well reported.

Extractive desulfurization (EDS) involves the selective extraction of sulfur compounds from fuel oils using a solvent or liquid-phase extraction process.[19−23] Although the process can be conducted under mild temperature conditions and without the use of a catalyst or hydrogen, proper selection of solvents to extract sulfur is a consuming task, as most of the solvents are volatile, making it difficult to reuse them. Biodesulfurization (BDS)[24,25] uses aerobic bacteria found in nature to remove sulfur heterocycles from petroleum without affecting the fuel value of the hydrocarbon matrix. However, there are two pathways for BDS, and one of them, the Kodama pathway, is slower than the other options. Additionally, it requires expensive microorganism development, which makes it unsuitable for industrial use due to its cost.

Oxidative desulfurization (ODS) is an alternative method that can be used with fuel oils instead of reductive HDS.[26−29] ODS avoids the use of hydrogen and can be carried out under milder reaction conditions. In this process, hydrogen peroxide (H_2O_2) is the most commonly used oxidizing agent, along with organic acids such as acetic acid (CH_3CO_2H) or formic acid (HCO_2H) to form the corresponding peroxy-organic acids (CH_3CO_3H or HCO_3H). The peroxy-organic acids oxidize the sulfur compounds into their corresponding sulfoxides or sulfones, which can then be more efficiently extracted with a suitable solvent extraction process. However, this process requires high loading of the oxidizing agent and large amounts of solvents, which are often volatile, flammable, and potentially environmentally hazardous, to selectively extract the oxidized products. Additionally, the organic acid catalysts can cause separation issues and are nonrenewable.

OEDS, on the other hand, is one of the feasible alternative options for the oil industry to eliminate sulfur compounds from fuel oils.[30−36] This technique involves using deep eutectic solvents for extraction and catalytic oxidation and is recognized for its environmentally friendly nature and mild reaction conditions. Nevertheless, the solvents used for the extraction can also dissolve in the fuel oils, resulting in both a loss of extractant and contamination of the fuel oil.

In recent years, ionic liquids (ILs),[37−56] have gained significant recognition and have become widely used in various fields of chemistry,[37,38] catalysis,[39] energy storage,[40] electrochemistry,[41] biomedical applications,[42] and drug delivery[43] as well as in the petroleum industry[33,34,45−56] for removal of sulfur-containing compounds from fuel oils. Ionic liquids (ILs) are typically defined as being low-melting-point salts having melting points below 100 °C, compared with traditional metal-nonmetal salts, which have much higher melting points. The cations and anions in typical ILs result in stable, low-volatility liquids with remarkable properties, making them versatile for numerous applications. The cations of ILs are generally stable heteroaromatic organic ions, such as the Lewis acid *N*-alkylated pyridinium or *N*-alkylated methylimidazolium cations. The most used inorganic anions are tetrafluoroborate (BF_4^-) or hexafluorophosphate (PF_6^-). Additionally, the counterions from the conjugate bases of weak and strong Brönsted acids, such as acetate ($CH_3CO_2^-$; Ac) and hydrogen sulfate (HSO_4^-), are also commonly utilized as anions in ILs. Compared with the other traditional desulfurization methods described previously, desulfurization using ILs shows the advantages of improved sulfur removal (S-removal) efficiency, having no requirement for hydrogen, and having low energy consumption. However, EDS with many ionic liquids still faces the challenges of high production cost of ILs and coextraction of the desired hydrocarbons. To improve the S-removal efficiency and reduce the simultaneous coextraction of hydrocarbons, coupled oxidative and extractive desulfurization (OEDS) processes using Lewis and Brönsted acidic ionic liquids (AILs) have been developed.[54−59] In this process, the AILs act as both extractants and catalysts, which are capable of first extracting the sulfur compounds from the oil phase into the ionic liquid phase and their oxides as their corresponding sulfones or sulfoxides when they have been oxidized in the presence of the oxidizing agent such as H_2O_2.[55] The most commonly used Lewis AILs include dialkylpyridinium tetrachloroferrates[56] and 1-octyl-3-methylimidazolium tetrachloroferrates [OMIm][$FeCl_4$].[57] Brönsted AILs that have been reported include *N*-methylimidazolium hydrogen sulfate [MIm][HSO_4], *N*-methylpyrrolidinium hydrogen sulfate [NMP][HSO_4],[58] [$HSO_3(CH_2)_4$MIm][HSO_4],[59] [$HCO_2(CH_2)_2$MIm][HSO_4],[60] *N*-carboxymethylpyridinium hydrogen sulfate [HCO_2CH_2Py][HSO_4], and *N*-carboxyethylpyridinium hydrogensulfate [$HCO_2(CH_2)_2$Py][HSO_4]).[61]

https://doi.org/10.1021/acsomega.3c09975
ACS Omega 2024, 9, 23485−23498

The main objectives of the study reported herein were to synthesize and characterize two new AILs and evaluate their catalytic performance in OEDS reactions, since the acetate anion in these AILs, unlike the hydrogen sulfate anion, is not acidic. The present study showed that ($[HO_2CCH_2Py][CH_3CO_2^-]$) (*N*-carboxymethylpyridinium acetate; **AIL1**) and $[HO_2C(CH_2)_2Py][CH_3CO_2][CH_3CO_2^-]$ (*N*-carboxyethylpyridinium acetate; **AIL2**) are very effective in removing sulfur compounds from a model diesel fuel. We have studied the effect of crucial factors, such as reaction temperature, H_2O_2 oxidant dosage, and the recycling of ILs and catalysts, on desulfurization efficiency. Furthermore, density-functional theory (DFT) computations were also conducted to understand how the present reported AILs interact with benzothiophene (BT), benzothiophene dioxide (BTO_2), dibenzothiophene (DBT), dibenzothiophene dioxide ($DBTO_2$), 4,6-dimethyl dibenzothiophene (4,6-DMDBT), and 4,6-dimethyl dibenzothiophene dioxide ($DMDBTO_2$). These calculations helped us to better understand the data gathered through our experiments.

2. MATERIALS AND METHODS

2.1. Materials. BT (98%), *n*-hexadecane (99%), 4,6-DMDBT (97%), and DBT (98%) were purchased from Alfa Aesar as model fuels. Additional reagents involving pyridine (99%), acetic acid (99.9%), chloroacetic acid (99%), ACS grade hydrogen peroxide (30%), and dichloromethane (99.5%) were purchased from Fisher Scientific.

2.2. Preparation of Ionic Liquids. *N*-Carboxymethylpyridinium acetate (**AIL1**) and *N*-carboxyethylpyridinium acetate (**AIL2**) were synthesized in a two-step process. The synthetic route for the acidic ionic liquids is shown in Scheme 1. The intermediate pyridinium chlorides ($[HO_2CCH_2Py][Cl^-]$ and ($[HO_2C(CH_2)_2Py][CH_3CO_2][Cl^-]$) were first prepared, and then 1:1 molar ratios of acetic acid were added dropwise to each of the intermediates with stirring. After reaction completion, the products formed were separated by vacuum filtration and washed three times with dichloromethane to remove all residual pyridine and then dried under a vacuum. The AILs were then stored in a fridge for further use.

*Synthesis of **AIL1**.* *N*-Carboxymethylpyridinium chloride was first synthesized by dissolving 2-chloroacetic acid (56.7 g, 0.6 mol) in deionized water (15.0 mL) in a three-necked round-bottomed flask. The solution was then agitated in an ultrasonic water bath at 15 °C for 10 min and pyridine (47.5 g, 0.6 mol) was then slowly added to the solution with agitation in the ultrasonic water bath. After the pyridine had been added, the mixture was allowed to react for a further 2 h. The water was removed from the reaction solution using rotary evaporation, and the resulting white precipitate was filtered and washed three times with dichloromethane to remove any remaining pyridine. The product was then dried in a vacuum-drying oven, yielding the colorless solid *N*-carboxymethylpyridinium chloride (65.2 g; 62.8%). In the second step, *N*-carboxymethylpyridinium chloride (17.4 g, 0.1 mol) was dissolved in 10.0 mL of deionized water in a three-necked round-bottomed flask. Acetic acid (98%, 6.0 g, 0.1 mol) was gradually introduced under comparable ultrasonic settings, and the mixture was left to react for 2 h. Following the completion of the reaction, rotary evaporation was employed to eliminate both hydrochloride acid and the unreacted acetic acid from the mixture, enabling the acquisition of 15.4 g (78%) of pure *N*-carboxymethylpyridinium acetate (**AIL1**) as evidenced by its ^1H and ^{13}C NMR spectra (Figures S1−S10).

*Synthesis of **AIL2**.* *N*-Carboxyethylpyridinium acetate (**AIL2**) was prepared using the same procedure as above, for **AIL1** by replacing 2-chloroacetic acid with the equivalent molar amount of 3-chloropropanoic acid in the first synthetic step. The final obtained product (15.4 g; 75%), *N*-carboxyethylpyridinium acetate **AIL2**, is a colorless viscous liquid.

2.3. Characterization of *N*-Carboxymethyl- and *N*-Carboxyethylpyridinium Acetates. The chemical structures of newly synthesized **AIL1** and **AIL2** were confirmed by their ^1H NMR (nuclear magnetic resonance), ^{13}C NMR, and Fourier-transform infrared (FTIR) spectra. The ^1H NMR and ^{13}C NMR spectra are presented in Figures S1−S10, and the FTIR spectra of the two AILs are displayed in Figures S11 and S12 in the Supporting Information (SI).

2.4. Oxidative and Extractive Desulfurization Experiments. Three model fuel oil solutions in *n*-hexadecane each having sulfur contents of 1000 mg/L were prepared using the appropriate amounts of the three sulfur heteroaromatic compounds DBT, BT, and 4,6-DMDBT. A typical OEDS experiment was conducted in a 50 mL round-bottom flask. Mixtures that contained 20.0 mL of model fuel oil and 1.20 mL of **AIL1** or **AIL2** were stirred at 40 °C for 20 min with the individual sulfur heteroaromatic compounds. Then, 0.27 mL of H_2O_2 (30 wt %) was added to each reaction mixture with stirring; after reaction completion, the mixtures were allowed to settle, and a separating funnel was used to separate the model fuel oil upper layer phase from the ionic liquid phase. The sulfur content of each of the upper oil phases (*n*-hexadecane) was analyzed by using high-performance liquid chromatography (HPLC). Additional experiments were conducted using different ratios of ionic liquid, model fuel, and H_2O_2 oxidant at varying temperatures (20, 30, and 40 °C) and with different extraction durations to determine the most efficient combination of these factors. Each experiment was conducted in duplicate.

2.5. Analytical Method of S-Containing Compounds. An Agilent 1260 HPLC system with a UV−vis detector and a ZORBAX Eclipse Plus C18 Rapid Resolution column (4.6 × 100 mm, 3.5 μm) was used to determine the concentration of S-compounds in the oil phase. The mobile phase consists of acetonitrile, water, and formic acid (85%: 15%: 0.1%, v/v/v). The parameters employed were a 1.0 mL/min flow rate, 10.00 μL injection volume, and 15.00 min elution time. All samples were filtered prior to the HPLC analysis. The amounts of S-compounds in the model fuel oils were determined by measuring the peak areas corresponding to the sulfur species identified by HPLC chromatography. Multistandard solutions containing BT, DBT, and 4,6-DMDBT in concentrations of 200.0, 150.0, 100.0, 75.0, 50.0, and 25.0 mg/L were prepared and analyzed at a wavelength of 284 nm to establish the concentration calibration curves for BT, DBT, and 4,6-DMDBT, which were then used to determine the contents of the S-compounds in the oil phase. The retention times for BT, DBT, and 4,6-DMDBT chromatograms were 1.674, 2.465, and 4.485 min, respectively.

2.6. Density Functional Theory (DFT) Calculations. To gain a better understanding of the interaction between the AILs and the S-containing compounds DBT, $DBTO_2$, BT, BTO_2, 4,6-DMDBT, and 4,6-$DMDTO_2$, a series of quantum chemical density functional theory (DFT) calculations[62] were

https://doi.org/10.1021/acsomega.3c09975
ACS Omega 2024, 9, 23485−23498

conducted using *Gaussian 16, Revision C.01*[63] at the ωB97XD/6-311++G(d,2p) level of theory. These calculations were performed in the gas phase as well as in *n*-hexadecane, *n*-hexane, and CCl_4 solvent systems, with the use of a polarized continuum model (PCM) at the ωB97XD/6-311++G(d,2p) level of theory. The initial molecular geometries of all the examined compounds were drawn using the *GaussView 6.0.16* program.[64] A vibrational frequency analysis was carried out for each optimized molecule to ensure that they had a minimum of vibrational energy and no imaginary frequencies. The structures of the *N*-carboxymethylpyridinium or *N*-carboxyethylpyridinium cations, $[HO_2CCH_2Py]$, and $[HO_2C(CH_2)_2Py]$ and their interactions with the acetate anion $[CH_3CO_2]$ at different bonding sites were optimized, and the most stable structures of the corresponding formed ionic liquid salts **AIL1** and **AIL2** were selected. The optimized structures of these ionic liquids were further optimized with the corresponding S-containing analytes (DBT, $DBTO_2$, BT, BTO_2, DMDBT, and $DMDBTO_2$). The binding interaction energy (ΔIE) values of the synthesized ionic liquids with the analytes were calculated from the electronic energies of the components by using eq 1.

$$\Delta IE = E_{[AIL]\supset[S-compound]} - (E_{[AIL]} + E_{[S-compound]}) \quad (1)$$

where $E_{[AIL]\supset[S\text{-compound}]}$ is the optimized energy of the AIL complex(es) with the S-compound; $E_{[AIL]}$ is the optimized electronic energy of the free AILs; and $E_{[S\text{-compound}]}$ is the optimized electronic energy of the individual S-compound (DBT, $DBTO_2$, BT, BTO_2, DMDBT, or $DMDBTO_2$).

3. RESULTS AND DISCUSSION

3.1. Characterization of AILs. The ^1H and ^{13}C NMR spectra of $[HO_2CH_2Py][Cl]$, **AIL1**, $[HO_2C(CH_2)_2Py][Cl^-]$ and **AIL2** are shown in Figures S1−S9, and their IR spectra for **AIL1** and **AIL2** are shown in Figures S11−S12.

AIL1: ^1H NMR (300 MHz, D_2O) (ppm): 8.34 (m, 2H, Py$H_{2,6}$), 8.12 (tt, m, J = 7.9, 1.6 Hz, 1H, PyH_4), 7.59 (m, 2H, 2H, Py$H_{3,5}$), 3.31 (t, J = 6.3 Hz, 2H, -CH_2Py), 2.29 (t, J = 6.3 Hz, 2H, -CH_2CH_2Py), 1.58 (s, 3H, -CH_3); ^{13}C NMR (75 MHz, D_2O) (ppm): 176.96, 176.52, 145.82, 141.55, 126.86, 40.31, 38.34, 20.81. 36 (m, 1H, PyH_4), 7.88 (m, 2H, 2H, Py$H_{3,5}$), 5.28 (s, 2H, −CH_2Py), 1.79 (s, 3H, -CH_3); ^{13}C NMR (75 MHz, D_2O): 176.24, 168.82, 146.63, 145.54, 127.99, 61.11, 20.43. The FTIR spectra (Figure S10) show the major peaks at wave numbers (cm^{-1}): 3442.31, 3061.30, 2612.11, 2520.51, 2006.57, 1724.64, 1694.24, 1638.23, 1490.70, 1380.78, 1247.72, 1013.11, and 898.66 cm^{-1}, both in the characteristic range for C−N stretching, as expected based on the structure of this **AIL1**.

AIL2: ^1H NMR (300 MHz, D_2O) (ppm): 8.34 (m, 2H, Py$H_{2,6}$), 8.12 (tt, m, J = 7.9, 1.6 Hz, 1H, PyH_4), 7.59 (m, 2H, 2H, Py$H_{3,5}$), 3.31 (t, J = 6.3 Hz, 2H, -CH_2Py), 2.29 (t, J = 6.3 Hz, 2H, -CH_2CH_2Py), 1.58 (s, 3H, -CH_3); ^{13}C NMR (75 MHz, D_2O) (ppm): 176.96, 176.52, 145.82, 141.55, 126.86, 40.31, 38.34, 20.81. The FTIR spectra (Figure S11) show the major peaks at wave numbers (cm^{-1}): 3455.81, 2923.56, 2850.27, 2604.39, 2465.54, 1750.08, 1688.37, 1617.91, 1466.60, 1293.04, 1230.36, 1171.54, 1070.30, 1005.7, 883.24, 851.4, 769.46, 613.25, and 575.65 cm^{-1}, both in the characteristic range for C−N stretching, as expected based on the structure of this **AIL2**.

3.2. Effect of the Carbon Chain Length and Acidity. The efficacy of the two newly developed AILs, **AIL1** and **AIL2**, was evaluated as catalysts and extractants for the removal of DBT from the model fuel using oxidation−extraction techniques. Figure 1 demonstrates that a minor quantity of DBT was extracted before the introduction of the oxidant (H_2O_2). Nevertheless, most of the sulfur was removed from the model fuel oil via the process of oxidation and extraction.

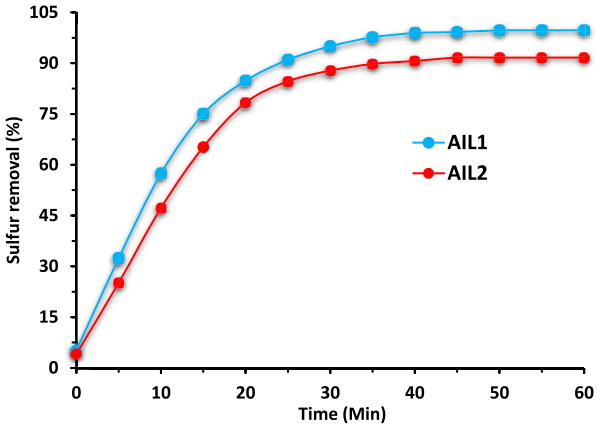

Figure 1. Effect of **AIL1** and **AIL2** on sulfur removal. Conditions: $V_{model\ fuel\ oil}$ (DBT) = 20 mL, V_{AILs} = 1.2 mL, T = 40 °C, and O/S = 6.

It is evident from Figure 1 that both AILs contributed significantly to the desulfurization process. The desulfurization process utilizing **AIL1** achieved a maximum efficiency of 99.8% after 40 min, while **AIL2** only obtained a desulfurization efficiency of 91.6%. The difference can be interpreted by comparing the acid strength characteristics of the two AILs. The pK_a values of the parent carboxylic acids in the respective ILs, namely, acetic acid and propionic acid, are 4.53 and 4.88, respectively, which is related to the chain length of the alkyl group. Thus, considering that the positive pyridinium ion is paired with the acetate anion counterion, it is reasonable to infer that the same trend for the Brønsted carboxylic acid portions of the respective AILs exists. This aligns with the experimental determinations of the acidity of the analogous hydrogen sulfate AILs that were reported by Zhang and co-workers.[61]

3.3. Structural Effect of the S-Containing Compounds. Figure 2a−c displays the chemical structures of DBT, 4,6-DMDBT, and BT, which were used as representative S-containing compounds to assess the desulfurization effectiveness of **AIL1** and **AIL2**.

The desulfurization efficiency may be influenced mainly by the aromatic π-electron density and electronic charge of the sulfur atoms in the molecules. It can be seen in Figure 2d−f that the electron density is highest surrounding the sulfur atoms of BT, DBT, and 4,6-DMDBT. The DFT-calculated electronic charges on the sulfur atom are −0.727, −0.781, and −1.015, respectively, as shown in Figure 2m−o. The molecular electrostatic surface potentials (ESPs) for DBT, 4,6-DMDBT, and BT are shown in Figure 2d−f. The color bar shows the relative polarities from the EPS values, which show the reactive sites of the species: negative EPS values are shown in red and the order of increasing electrostatic potentials is red > orange > yellow > green > blue. Otsuki et al.[65] reported electron densities of BT, DBT, and 4,6-DMDBT as 5.739, 5.758, and 5.760 e $Å^{-3}$, respectively, which is in agreement with the trend

https://doi.org/10.1021/acsomega.3c09975
ACS Omega 2024, 9, 23485−23498

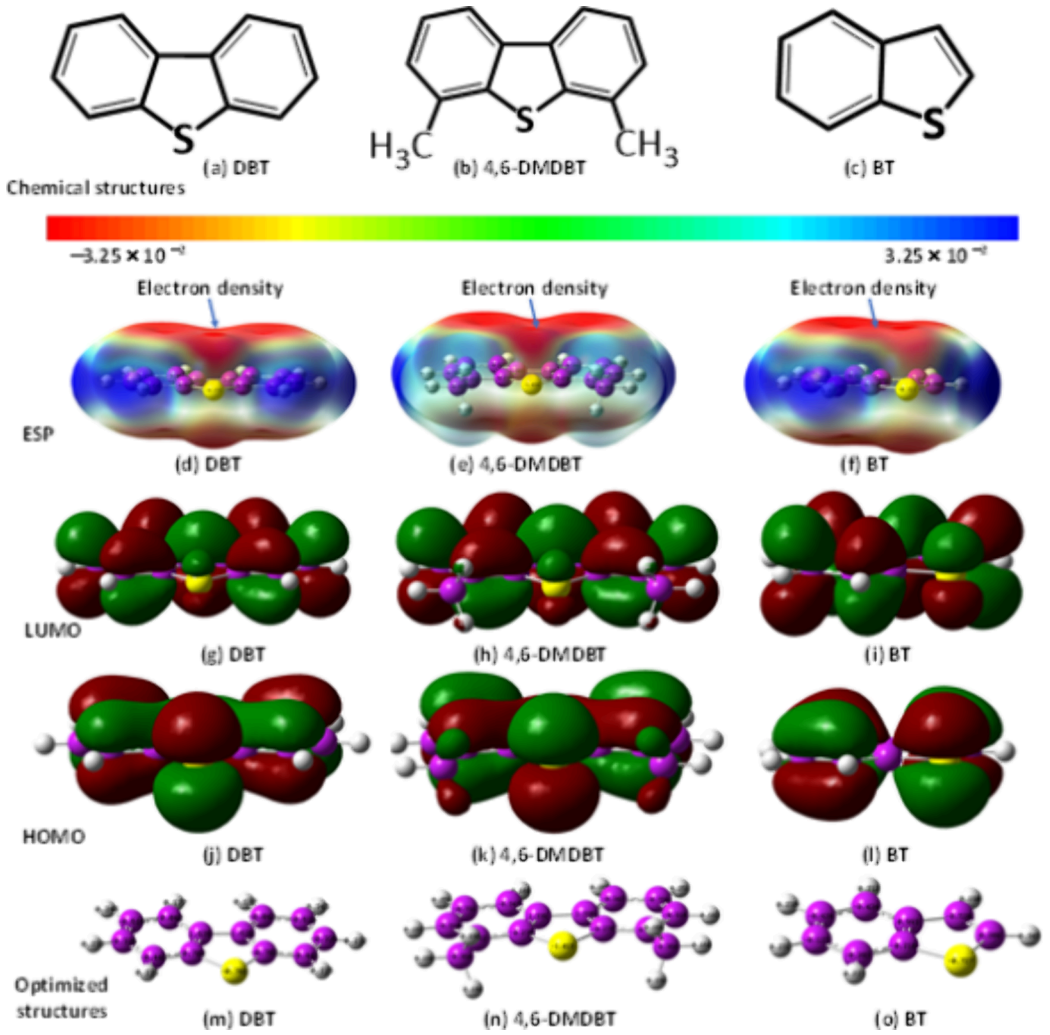

Figure 2. Chemical structures (a–c); DFT-calculated optimized frontier molecular orbital structures of ESP (d–f), LUMOs (g–i), HOMOs (j–l), and optimized (m–o) structures of DBT, 4,6-DMDBT, and BT at the ωB97XD/6-311++G(d,2p) level of theory in the *n*-hexadecane solvent system. Color code: carbon: purple; hydrogen: white; nitrogen: blue; oxygen: red; sulfur: yellow.

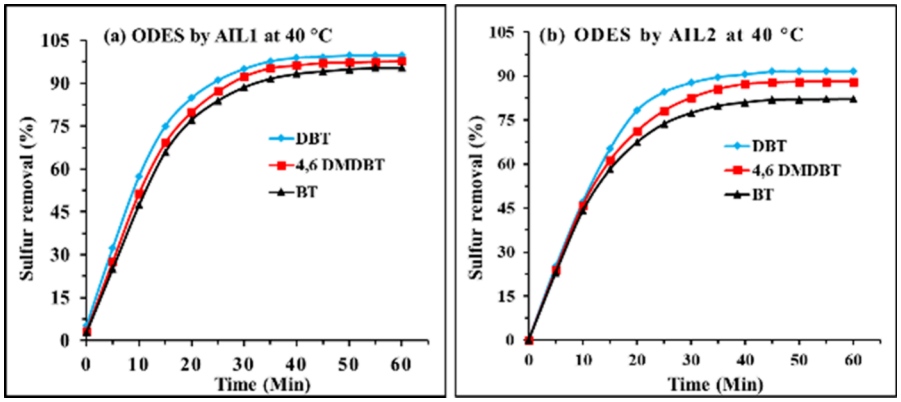

Figure 3. Extraction kinetics of DBT, 4,6-DMDBT, and BT by **AIL1** (a) and **AIL2** (b) from model fuel oils. $V_{\text{model fuel oil}}$ = 20.0 mL, V_{AIL} = 1.20 mL, T = 40 °C, O/S = 6.

observed above by us for the electronic charges on the S atoms using a higher-level basis set. As noted by Otsuki et al., there is a positive correlation between the rate of oxidation, i.e., 4,6-DMDB > DBT > BT, with the magnitude of the electron density on the respective sulfur atoms.[65] Although experimentally it was found that 4,6-DMDBT is more easily oxidized than DBT, DBT exhibits a significantly greater desulfurization capacity when compared with 4,6-DMDBT. The reason proposed for the low efficiency in extracting 4,6-DMDBT is due to the presence of the methyl substituents at the 4 and 6 positions of DBT, which inductively enhances the electron

https://doi.org/10.1021/acsomega.3c09975
ACS Omega 2024, 9, 23485−23498

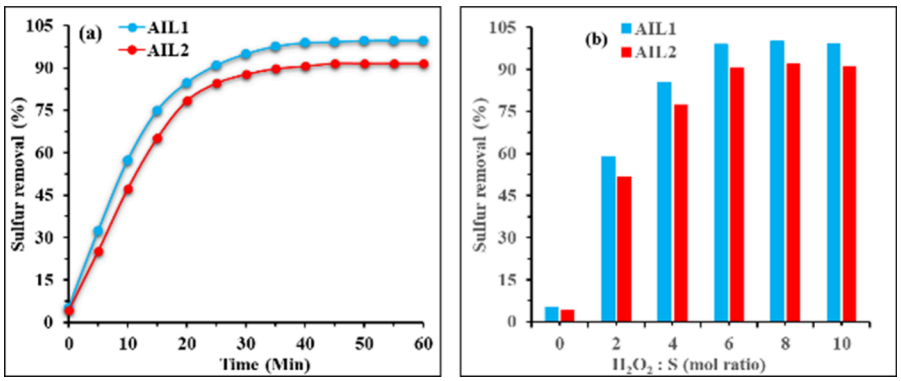

Figure 4. Removal rate (a) and effect of H_2O_2 dosage (b) on the DBT-removal efficiency from the model fuel oil (*n*-hexadecane). $V_{\text{model fuel oil}}$ = 20 mL, V_{AIL} = 1.2 mL, T = 40 °C.

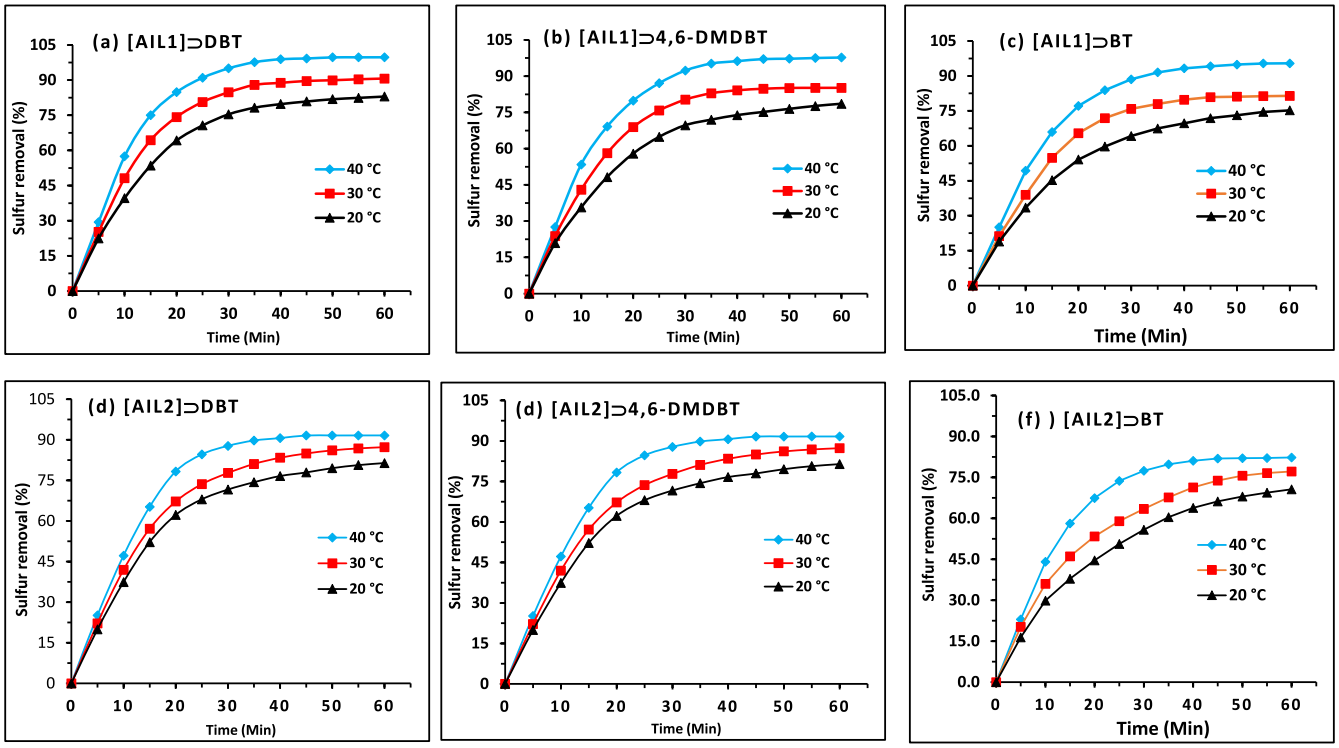

Figure 5. Effect of temperatures and reaction time for sulfur removal rates (%) of DBT, 4,6-DMDBT, and BT in model fuel oil (*n*-hexadecane) with **AIL1** (a–c) and **AIL2** (d–f) at 20, 30, and 40 °C.

density on the S atoms and provides steric hindrance, limiting the ability of 4,6-DMDBT to access the ionic liquids.[65]

The experimental results demonstrate that the desulfurization efficiency using **AIL1** and **AIL2** follows the subsequent order: DBT > 4,6-DMDBT > BT as depicted in Figure 3. The three S-compounds demonstrate similar patterns in extraction kinetics. At first, there was a rapid increase in the sulfur removal rate of the model fuel oils. After 40 min, the rate of removal started to level off. Within 60 min, **AIL1** extracted 99.8% of DBT, 97.8% of 4,6-DMDBT, and 95.4% of BT (Figure 3a), while **AIL2** achieved removal efficiencies of 91.6% for DBT, 87.3% for 4, 6-DMDBT, and 82.4% for BT (Figure 3b).

3.4. Effect of the H_2O_2 Dosage. To investigate the effect of the H_2O_2 dosage on the S-removal efficiency by **AIL1** and **AIL2**, DBT was used in the model fuel oil with varied molar ratios of H_2O_2:S (O/S). The rate and efficiency of desulfurization are undoubtedly affected by the amount of H_2O_2 employed. H_2O_2 is believed to produce peroxy carboxylic acid moieties of **AIL1** and **AIL2**, resulting in the synthesis of $[HO_3CCH_2Py][CH_3CO_2]$ and $[HO_3C(CH_2)_2Py][CH_3CO_2]$. The peroxy acid AILs are believed to be the oxidants of sulfur compounds. Figure 4a displays the DBT removal rate, while Figure 4b presents a histogram demonstrating the impact of the H_2O_2 dosage on the effectiveness of desulfurization. In the absence of H_2O_2, only a minimal proportion of DBT in the fuel oil phase is removed at a temperature of 40 °C during the 40–60 min reaction period(s). The desulfurization rate is directly proportional to the dosage of the H_2O_2 oxidant. Nevertheless, under the temperature of 40 °C, the optimum O/S ratio was determined to be 6, resulting in a DBT removal rate of 99.75%.

3.5. Temperature and Reaction Time Effects. The effectiveness of OEDS for a particular fuel oil is greatly

https://doi.org/10.1021/acsomega.3c09975
ACS Omega 2024, 9, 23485–23498

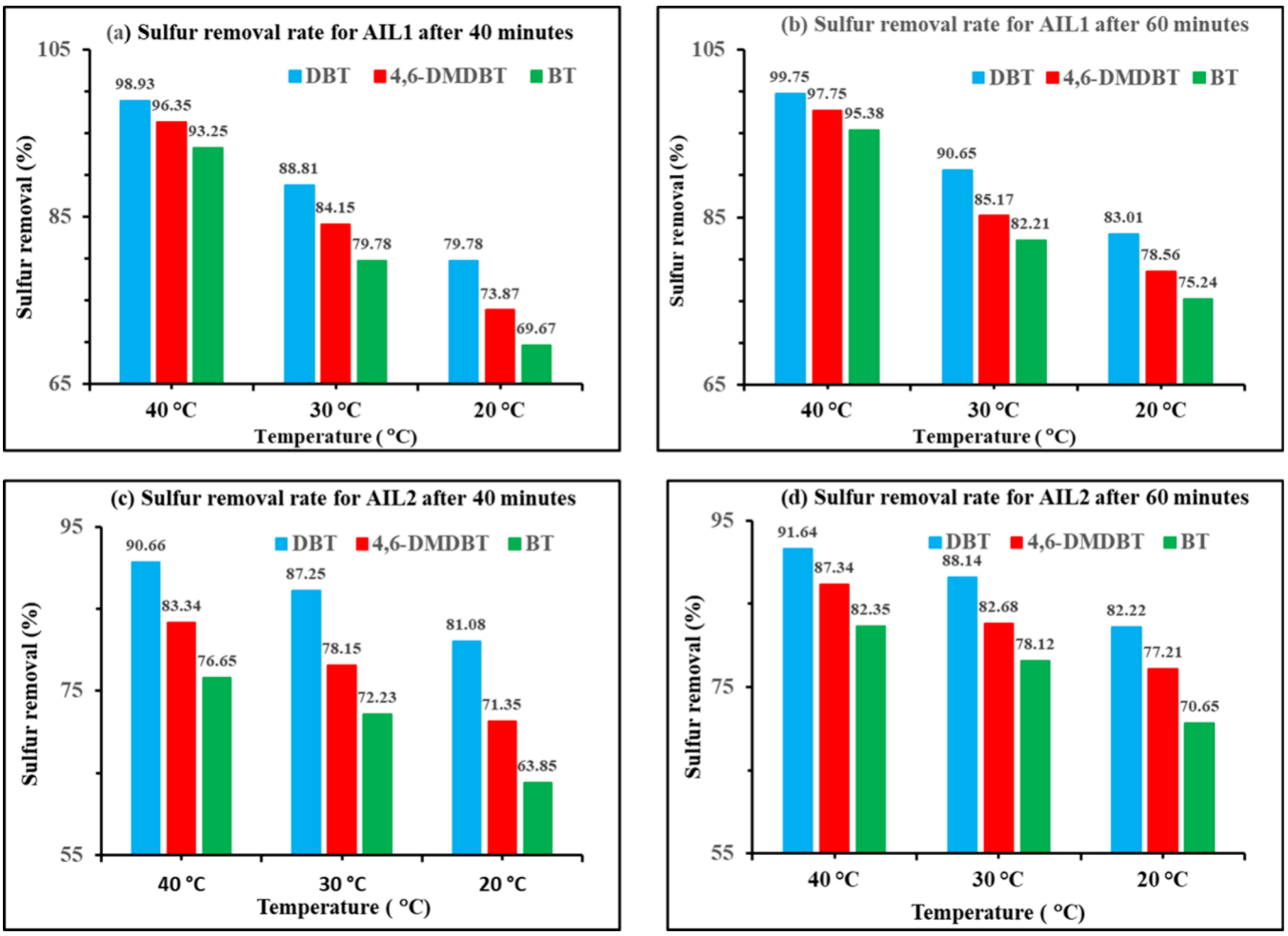

Figure 6. Histogram showing the percentage of sulfur removal for DBT, 4,6-DMDBT, and BT in the model fuel oil (*n*-hexadecane) using **AIL1** (a, b) and **AIL2** (c, d) at 20, 30, and 40 °C after 40 and 60 min.

influenced by the reaction temperatures and durations. The sulfur removal from the *n*-hexadecane (model fuel oil) with **AIL1** and **AIL2** was investigated at different temperatures (20, 30, and 40 °C) and for reaction periods of 40 and 60 min, with the optimal O/S molar ratio of 6. Figures 5 and 6 illustrate the impact of the temperature on the removal of DBT, BT, and 4,6 DMDBT from the model fuel with the reaction temperature varying from 20 to 40 °C. The removal rates of DBT, 4,6-DMDBT, and BT from the model fuel oil (Figure 5a–f) increase rapidly with both AILs initially. However, after 40 min, the rates gradually stabilize and attain steady-state plateaus. The order of extent of desulfurization is DBT > 4, 6-DMDBT > BT. After 60 min, **AIL1** retrieved 99.8% of DBT, 97.8% of 4,6-DMDBT, and 95.4% of BT at 40 °C. A trend similar to that was observed with **ALI2**. The sulfur removal efficiency values for DBT, 4,6-DMDBT, and BT by **AIL2** at a temperature of 40 °C after 60 min are 91.6%, 87.3%, and 82.4%, respectively.

As shown in Figure 6a–d, the sulfur removal rate increases with rising temperature. According to Figure 6a, at a temperature of 40 °C and after a duration of 40 min, the rates of sulfur removal for DBT, 4,6-DMDBT, and BT by **AIL1** were 98.9%, 96.4%, and 93.2%, respectively. However, the removal rates of DBT, 4,6-DMDBT, and BT at a temperature of 20 °C were only 79.78%, 73.87%, and 69.67%, respectively. The desulfurization efficiency using **AIL2** showed similar outcomes, as seen in Figure 6c,d. These findings suggest that the optimal temperature of 40 °C is sufficient to remove the S-compounds from model fuel oil using an OEDS process. The efficiency and rate of desulfurization are directly proportional to the rise in temperature, regardless of the ionic liquid type employed.

3.6. DFT Studies. To investigate the interactions between acid ionic liquids and the heteroaromatic S-containing compounds DBT, 4,6-DMDBT, BT, and their corresponding dioxides, $DBTO_2$, 4,6-$DMDTO_2$, and BTO_2, a quantum chemical density functional theory (DFT) study[62] was carried out using *Gaussian 16, Revision C.01*[63] at the ωB97XD/6-311++G(d,2p) level of theory. The interactions between two or more molecular species are dependent on the cumulative effects of weak intermolecular forces, such as electrostatic, hydrogen bonding, π–π, and hydrophobic-lipophilic interactions. These are the intermolecular forces that enable ILs to effectively bind with and thereby remove polar sulfur-containing compounds from diesel and fuel oils. The DFT calculations were initially performed in the gas phase followed by performing the calculations in model *n*-hexadecane, *n*-hexane, and CCl_4 solvent systems using a polarized continuum model (PCM). The energetically most stable optimized structures, ESP, LUMOs, and HOMOs structures of **AIL1** and **AIL2**, DBT, $DBTO_2$, and their 1:1 hypothetical supramolecular complexes are shown in Figures 7–10. The DFT-

https://doi.org/10.1021/acsomega.3c09975
ACS Omega 2024, 9, 23485–23498

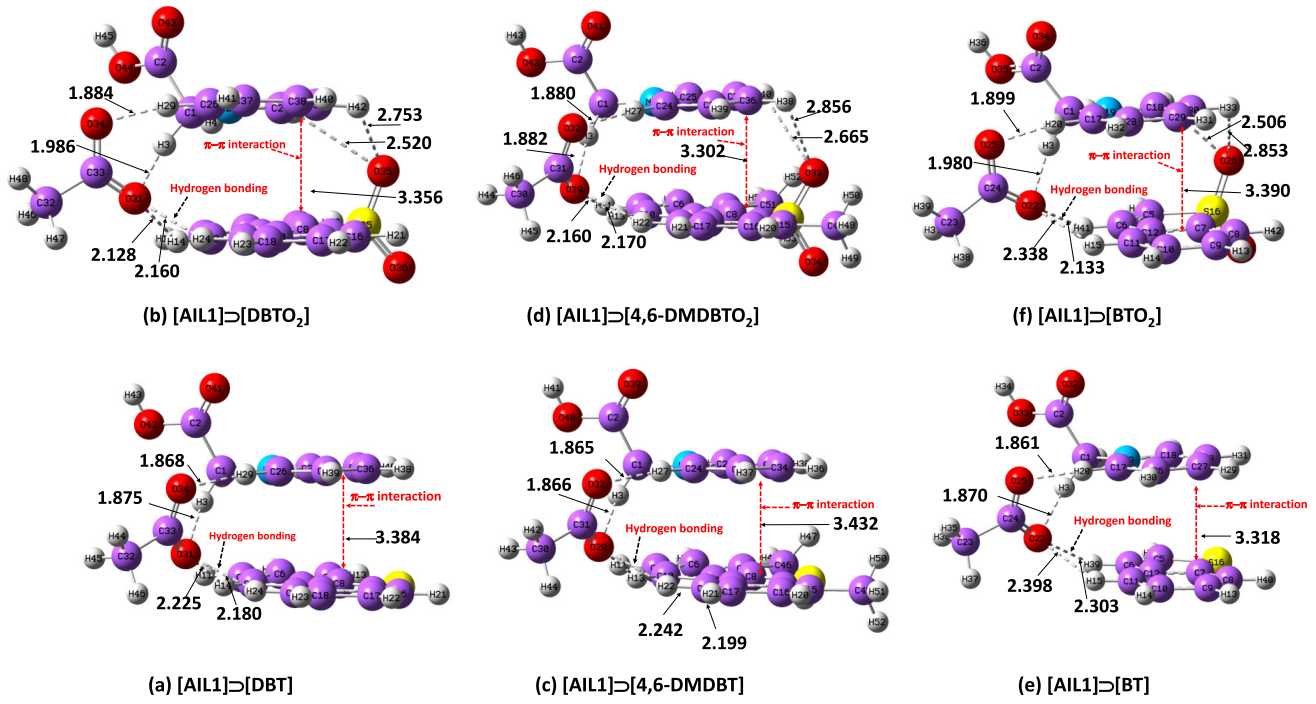

Figure 7. Optimized DFT gas phase hypothetical molecular *face-to-face parallel sandwich* structures of the 1:1 **AIL1** complexes with DBT (a), $DBTO_2$ (b), 4,6-DMDBT (c), 4,6-$DMDBTO_2$ (d), BT (e), and BTO_2 (f) at the ωB97XD/6-311++G(d,2p) level of theory (color code: carbon: purple; hydrogen: white; nitrogen: blue; oxygen: red; sulfur: yellow).

calculated electronic binding interaction energies (ΔIE kJ/mol) are summarized in Table 1. Negative ΔIE (kilojoules per mole) values correlate with more favorable interactions. The DFT-calculated results confirm that **AIL1** has slightly higher electronic binding interaction energies than **AIL2** for the 1:1 complexes in the following order: DBT > 4,6-DMDBT > BT, and in the same order for their corresponding sulfone compounds, i.e., $DBTO_2$ > 4,6-$DMDBTO_2$ > BTO_2. The dioxides or sulfone compounds show higher negative ΔIE (kJ/mol) values compared with their precursor compounds due to their higher polarity and the consequential additional hydrogen bonding that can form between oxygen atoms and the sulfonyl groups with the most electron-deficient H-atoms on the pyridine rings of the AILs (see top rows of Figures 6 and 7). The DFT-calculated selected bond distances (in angstroms (Å)) for the selected atoms for the 1:1 complexes of the ILs with the S-containing compounds reported in Table 2 show that the sulfone compounds have shorter intermolecular bond distances. This agrees with the presumed more favorable interactions between the ionic liquids with the sulfones as compared with their unoxidized S-compounds.

Table 1. DFT-Calculated Electronic Binding Interaction Energies (ΔIE kJ/mol) for the Hypothetical 1:1 Supramolecular Complexes of AIL1 and AIL2 with DBT, $DBTO_2$, BT, BTO_2, DMDBT, and 4,6-$DMDBTO_2$ at the ωB97XD/6-311++G(d,2p) Level of Theory in the Gas Phase and in *n*-Hexane, *n*-Hexadecane, and CCl_4 Solvent Systems

	electronic interaction energies (ΔIE kJ/mol)			
complexes	gas phase	hexane	hexadecane	CCl_4
AIL1⊃DBT	−93.09	−76.62	−75.14	−73.64
AIL2⊃DBT	−90.48	−74.67	−73.69	−72.15
AIL1⊃$DBTO_2$	−105.10	−86.71	−84.75	−82.74
AIL2⊃$DBTO_2$	−103.56	−85.76	−83.00	−81.49
AIL1⊃4,6-DMDBT	−90.92	−75.38	−74.50	−72.60
AIL2⊃4,6-DMDBT	−89.57	−74.15	−75.27	−70.84
AIL1⊃4,6-$DMDBTO_2$	−104.04	−85.72	−83.92	−82.08
AIL2⊃4,6-$DMDBTO_2$	−103.20	−84.94	−82.63	−80.76
AIL1⊃BT	−73.34	−60.89	−59.73	−58.55
AIL2⊃BT	−74.15	−59.15	−58.43	−57.16
AIL1⊃BTO_2	−96.35	−75.92	−73.90	−71.84
AIL2⊃BTO_2	−95.35	−74.00	−72.46	−70.34

Figure 7a shows the energy-optimized structure of the hypothetical 1:1 **AIL1**⊃[DBT] supramolecular complex to be in a *face-to-face parallel-sandwich*-type arrangement, with two hydrogen bonding interactions from the pyridinium cation to the closest acetate anion's oxygen atoms, having bond distances of 1.884 and 1.986 Å. Similarly, the DBT component also has the closest hydrogen bond contacts with the acetate anion's oxygen atoms at bond distances of 2.180 and 2.225 Å. Furthermore, the plane of the pyridinium ring is parallel to that of the DBT plane, separated by 3.384 Å due to the $\pi-\pi$ interactions between the two rings. Similar hydrogen bonding interactions and $\pi-\pi$ interactions between the pyridine ring of **AIL1** can also be observed in the 1:1 **AIL1**⊃[4,6-DMDBT] and **AIL1**⊃[BT] complexes as shown in Figure 7c,e, respectively. Figure 7b,d,f shows the 1:1 complexes of **AIL1**⊃[$DBTO_2$], **AIL1**⊃[4,6-$DMDBTO_2$], and **AIL1**⊃[BTO_2], all of which are arranged in similar *face-to-face parallel sandwich* energy-optimized structures.

Figure 7b presents two hydrogen bonding interactions in the energy-optimized hypothetical supramolecular **AIL1**⊃[$DBTO_2$] complexes from the pyridinium cation to the closest oxygen atom of the acetate anion, with bond distances of 1.884 and 1.986 Å. The $DBTO_2$ also has similar pyridinium cation-acetate bond distances of 2.128 and 2.160 Å. The pyridinium ring plane is parallel to that of the DBT plane, separated by

https://doi.org/10.1021/acsomega.3c09975
ACS Omega 2024, 9, 23485−23498

Table 2. DFT-Calculated Selected Bond Distances (in Ångstroms (Å)) for Selected Atoms from the Energy-Optimized 1:1 Complexes of AIL2 and AIL2 with DBT, $DBTO_2$, BT, BTO_2, DMDBT, and 4,6-$DMDBTO_2$ at the ωB97XD/6-311++G(d,2p) Level of Theory in the Gas Phase

	selected atom bond distances (Å)		
complexes	pyridine ring to S-compounds	(O---H)[a]	(>S═O···H)[b]
AIL1⊃DBT	3.384	2.180/2.225 *(Avg. 2.202)*	
AIL2⊃DBT	3.381	2.161/2.220 *(Avg. 2.19)*	
AIL1⊃$DBTO_2$	3.356	2.128/2.160 *(Avg. 2.144)*	2.52/2.753 (Avg. 2.263)
AIL2⊃$DBTO_2$	3.311	2.118/2.136 *(Avg. 2.123)*	2.687/2.80 (Avg. 2.274)
AIL1⊃4,6-DMDBT	3.432	2.242/2.199 *(Avg. 2.220)*	
AIL2⊃4,6-DMDBT	3.401	2.172/2.240 *(Avg. 2.206)*	
AIL1⊃4,6-$DMDBTO_2$	3.302	2.160/2.170 *(Avg. 2.202)*	2.665/2.856 (Avg.2.760)
AIL2⊃4,6-$DMDBTO_2$	3.311	2.133/2.149 *(Avg. 2.141)*	2.695/2.767 (Avg. 2.731)
AIL1⊃BT	3.318	2.303/2.398 *(Avg. 2.333)*	
AIL2⊃BT	3.319	2.299/2.364 *(Avg. 2.331)*	
AIL1⊃BTO_2	3.390	2.133/2.338 *(Avg. 2.235)*	2.506/2.853 (Avg. 2.679)
AIL2⊃BTO_2	3.412	2.136/2.319 *(Avg. 2.227)*	2.483/2.894 (Avg. 2.688)

[a]Note: Distance between acetyl oxygen of the ionic liquids and closest H of DBT, $DBTO_2$, 4,6- DMDBT, 4,6-DMDBTO2, BT, and BTO_2. [b]Distance between sulfone oxygen of the S-compounds and closest H atom of the pyridine ring.

3.356 Å due to the π−π interaction between the two rings. Furthermore, this complex shows two additional hydrogen bonds between the sulfonyl group's oxygen atoms and the closest pyridine ring hydrogen atom with bond distances of 2.520 and 2.753 Å. These also contribute to the formation of energetically more favorable structures. According to the findings presented in Figure 7d,f, it is apparent that the Brønsted acid **AIL1** displays a significant affinity toward forming stronger 1:1 complexes with both [4,6-$DMDBTO_2$] and [BTO_2]. The DFT-calculated selected bond distances (in angstroms (Å)) for the 1:1 supramolecular complexes of **AIL1** and **AIL2** with the S-containing compounds are summarized in Table 2.

The corresponding energy-optimized hypothetical supramolecular 1:1 complexes of Brønsted acid **AIL2** with DBT, $DBTO_2$, 4,6-DMDBT, 4,6-$DMDBTO_2$, BT, and BTO_2 are illustrated in Figure 8. It was found that both acidic ionic liquids could be able to form strong hydrogen bonding and π−π interactions with the selected S-compounds, thus providing further insight into their chemical properties and potential applications. Both ionic liquids exhibit higher interaction energies (ΔIE) with the oxidized sulfone compounds compared with their precursor S-compounds (Table 1).

To gain a better understanding of the nature of the interactions between specific ionic liquids (ILs) in general and different organic sulfur compounds, it is essential to consider their DFT-computed stabilities and molecular interaction energies (ΔE_{INT}). These are based upon the most stable geometries generated for these molecules and their respective frontier molecular orbitals (FMOs),[66] which are their highest occupied molecular orbitals (HOMOs) in which their electrons are located, and their lowest unoccupied molecular orbitals (LUMOs). According to Koopmans' theorem, the energy levels of HOMOs and LUMOs are related to their nucleophilic and electrophilic properties, respectively.[67] Large HOMO−LUMO gaps signify high stability and low reactivity of the chemical species.

The HOMO−LUMO energy values shown in Tables S1 and S2 (Supporting Information) can be used to calculate several other significant and valuable quantum chemical properties such as global hardness (η), global softness (S), electrophilicity index (ω), electronegativity (χ), and chemical potential (μ), which all measure chemical reactivity.[68,69] These were

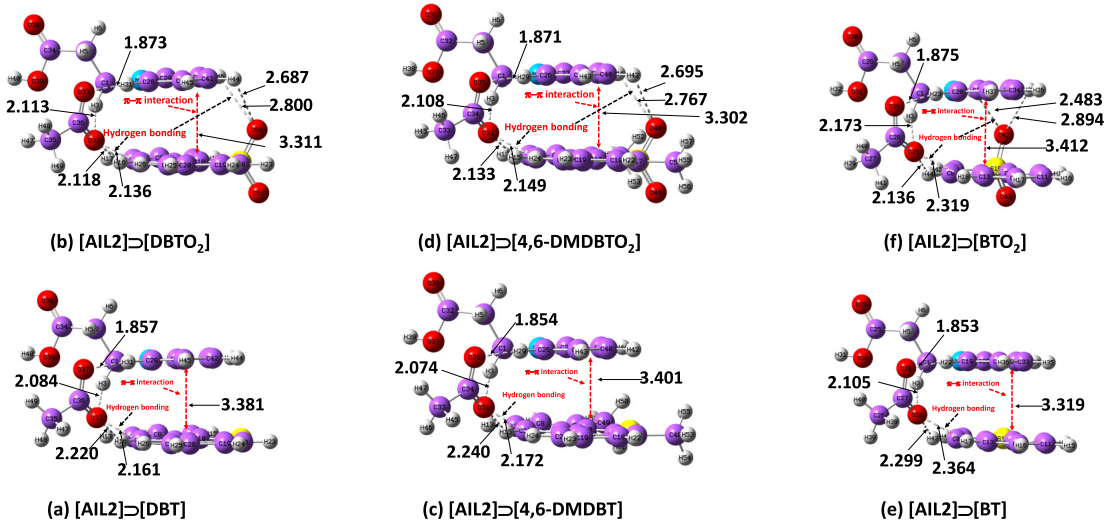

Figure 8. Optimized gas phase hypothetical molecular *face-to-face parallel sandwich* structures of the 1:1 complexes of **AIL2** with DBT (a), $DBTO_2$ (b), 4,6-DMDBT (c), 4,6-$DMDBTO_2$ (d), BT (e), and BTO_2 (f) at the ωB97XD/6-311++G(d,2p) level of theory (color code: carbon: purple; hydrogen: white; nitrogen: blue; oxygen: red; sulfur: yellow).

https://doi.org/10.1021/acsomega.3c09975
ACS Omega 2024, 9, 23485−23498

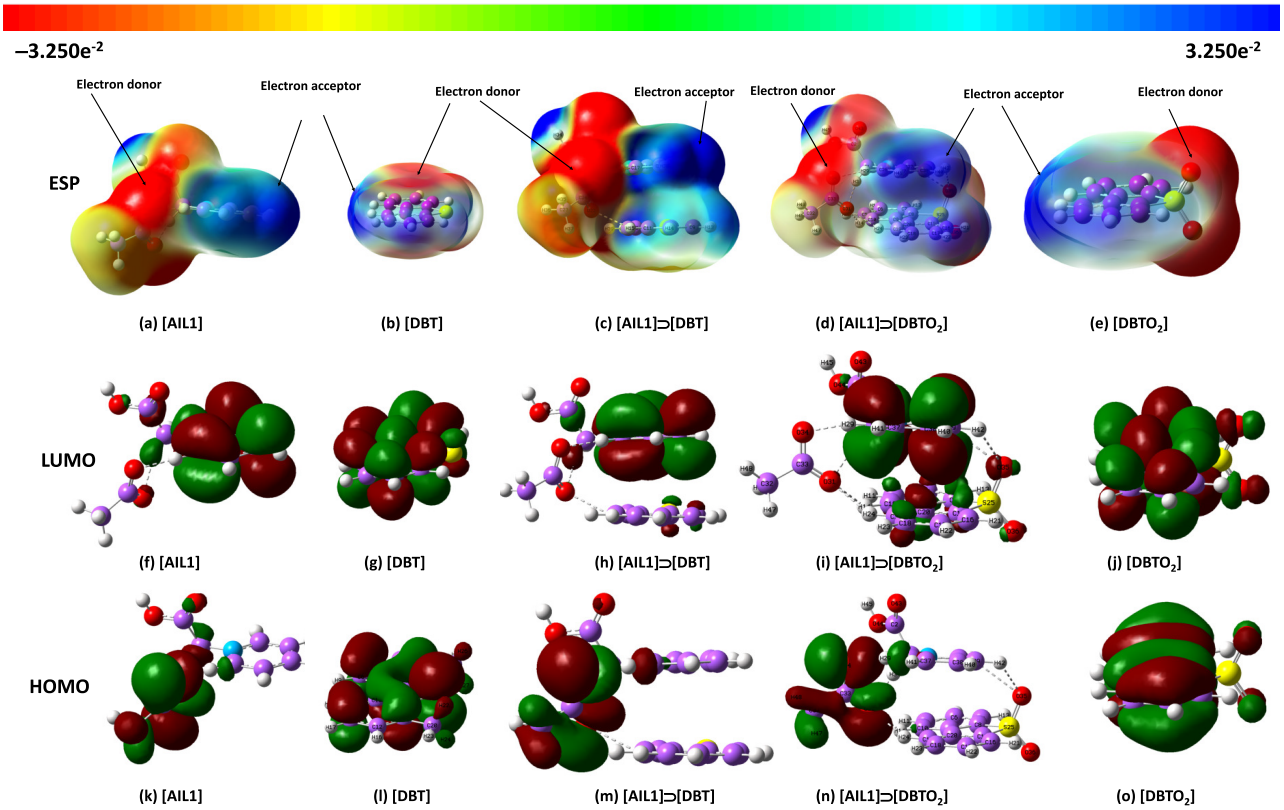

Figure 9. DFT-calculated optimized frontier molecular orbital structures of ESP (a−e), LUMOs (f−j), and HOMOs (k−o), structures of **AIL1** and its 1:1 complexes with DBT and $DBTO_2$ at the ωB97XD/6-311++G(d,2p) level of theory in the *n*-hexadecane solvent system. Color code: carbon: purple; hydrogen: white; nitrogen: blue; oxygen: red; sulfur: yellow.

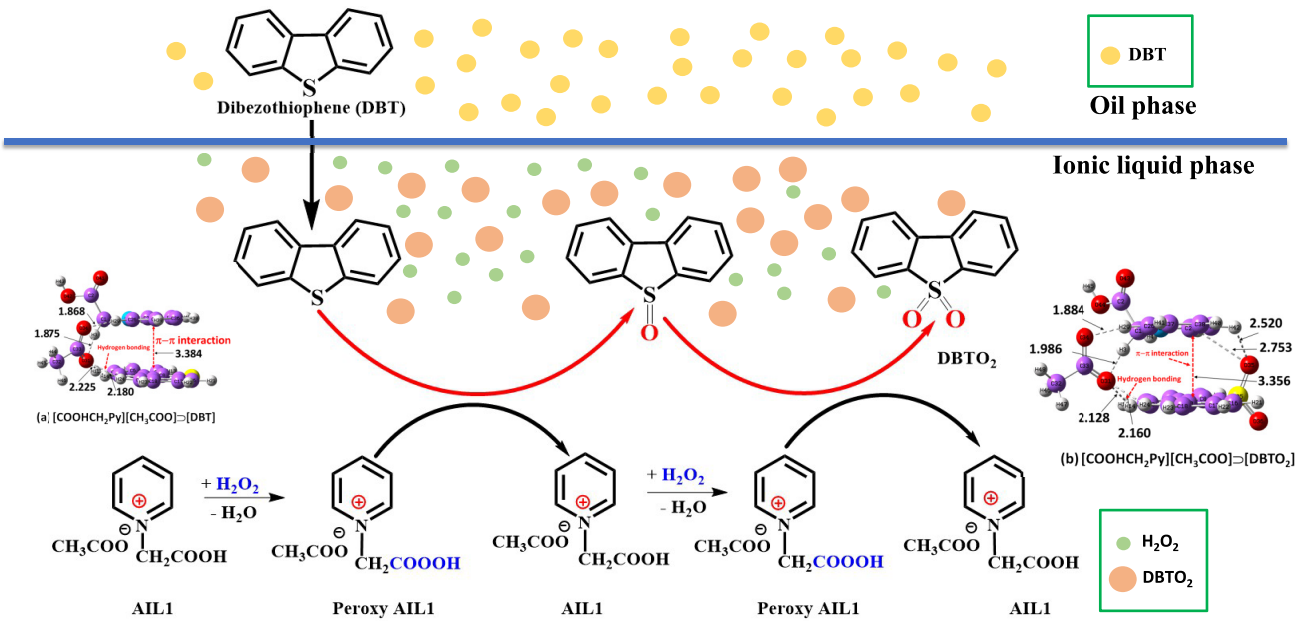

Figure 10. Proposed hypothetical reaction mechanism for the OEDS removal of DBT from a fuel oil using as an example, the acidic ionic liquid *N*-carboxymethyl pyridine acetate **AIL1**.

generated using the *GaussView 6.0.16* software, and the surfaces were formed by mapping the electrostatic potentials (EPs)[70−72] onto their HOMO electron density surfaces. The EPs show the relative polarities and thus the reactive sites of the species: the negative EPs are shown in red and the order of increasing electrostatic potentials (i.e., highest negative value) is red > orange > yellow > green > blue. Figure 9 shows that the hydrogen atoms in pyridine, DBT, and $DBTO_2$ rings are the most nucleophilic sites, which tend to interact with the electrophilic CH_3COO^- anion of ionic liquid **AIL1**. Figure 9 shows HOMOs, LUMOs, and molecular electrostatic surface potential (ESP)[68,69] maps of **AIL1** and its 1:1 hypothetical

https://doi.org/10.1021/acsomega.3c09975
ACS Omega 2024, 9, 23485−23498

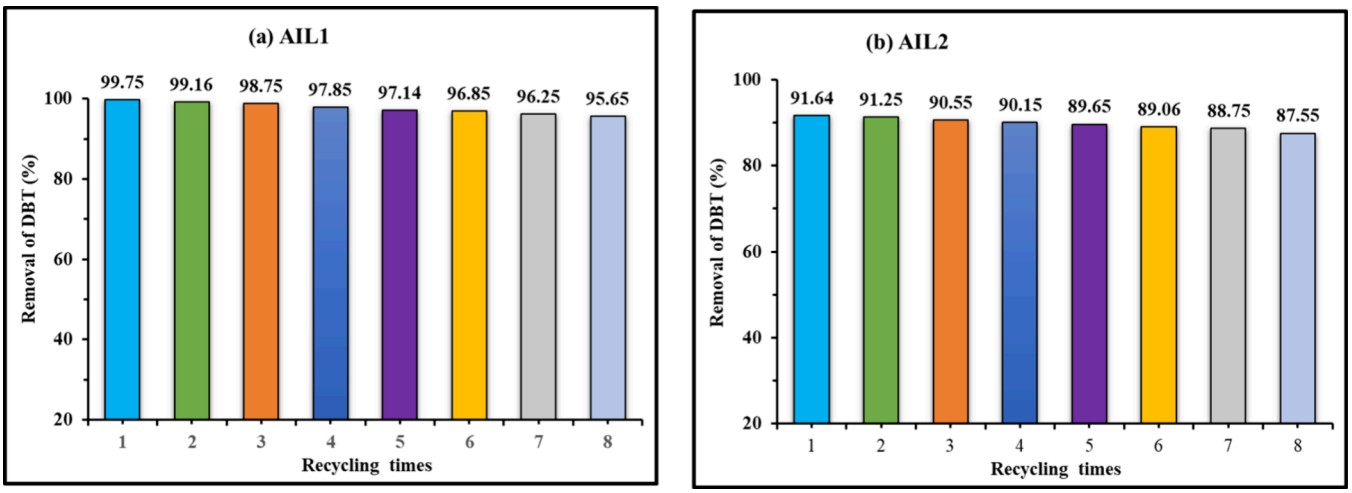

Figure 11. Reusability of **AIL1** (a) and **AIL2** (b) for DBT removal from model fuel oil (*n*-hexadecane) under the following condition: $V_{\text{model fuel oil}}$ = 20 mL, V_{AIL} = 1.2 mL, T = 40 °C, and O/S= 6.

complexes with DBT and $DBTO_2$**AIL1**⊃[DBT] and **AIL1** ⊃[$DBTO_2$]), respectively. The surfaces were formed by mapping the electrostatic potentials (MESPs) onto their HOMO electron density surfaces. The ESPs show the relative polarities and thus the reactive sites of the species: the negative ESP values are shown in red, and the order of increasing electrostatic potentials (i.e., highest negative value) is red > orange > yellow > green > blue.

3.7. Possible Mechanism for the Extraction−Oxidation Desulfurization Process. To elucidate the potential reaction mechanism, DBT was selected as a representative sulfur compound for the oxidation-extraction process, **AIL1** was utilized as the extractant and catalyst, and H_2O_2 served as the oxidant. It is postulated that **AIL1** facilitates the transfer of the DBT compound from the oil phase to the ionic liquid phase.

Figure 10 depicts a possible reaction process for OEDS of DBT using **AIL1** and H_2O_2. The process is achieved through the $\pi-\pi$ interaction between the pyridine ring and the acetate anion's hydrogen bonding interaction with the closest DBT hydrogen. DFT calculated the *face-to-face* interaction between **AIL1** and DBT, with the ball and stick structure shown on the left side image in Figure 10. When H_2O_2 is introduced to the OEDS process of DBT, the acidic ionic liquid **AIL1** undergoes a chemical reaction and transforms it into the highly reactive peroxy acid $[HO_2CCH_2Py][CH_3CO_2]$. This newly formed peroxy acid is a more potent oxidizing agent capable of transforming DBT into its respective sulfoxide (DBTO) and sulfone ($DBTO_2$). The formation of a stable $DBTO_2$-AIL1 complex was observed, as illustrated in the figure on the right-hand side of Figure 10.

3.8. Regeneration of AIL1 and AIL2. Ionic liquids have diverse uses across multiple fields in industrial processes but are relatively expensive. Hence, it is crucial to prioritize the recycling and regeneration of ionic liquids to achieve sustainability and efficiency goals. In this work, the used AILs were regenerated first by rotary evaporation, which involved the removal of water and the remaining H_2O_2. Subsequently, the oxidation byproducts of the sulfur compounds present in the AILs were extracted by carbon tetrachloride (CCl_4). The regenerated ionic liquids, **AIL1** and **AIL2**, underwent analysis for their purity using ^{1}H NMR, ^{13}C NMR, and FT-IR spectroscopy after being dried under a vacuum. The results indicated that the AILs remained fundamentally unchanged from their initial state before the extractions. In other words, there were no alterations in the composition and structures of the acid ionic liquids. The regenerated ionic liquids were employed for the subsequent OEDS process. Figure 11 demonstrates the effect of using recycled ionic liquids on desulfurization efficiency. Based on our investigation, both **AIL1** (Figure 11a) and **AIL2** (Figure 11b) can be reused up to nine times without a significant decrease in their effectiveness in removing sulfur compounds from the model fuel. Overall, this study illustrates the potential of regenerating and recycling ionic liquids to facilitate efficient and ecologically sustainable industrial processes.

4. CONCLUSIONS

In this study, two new acidic ionic liquids, *N*-carboxymethylpyridinium acetate (**AIL1**) and *N*-carboxyethylpyridinium acetate (**AIL2**), were synthesized and then were used for the removal of BT, DBT, and 4,6-DMDBT from a model fuel oil (*n*-hexadecane). The experimental results showed that both ionic liquids have higher desulfurization rates at 40 °C. **AIL1** showed a higher sulfur (i.e., DBT) removal rate compared with **AIL2**, and it reached 99.8% when 1.2 mL of the IL was used with 20 mL of the model fuel oil and with an H_2O_2/sulfur molar ratio of 6 and a reaction time of 60 min at 40 °C. Acidic ionic liquids can be regenerated and reused up to 9 times without a significant decline in desulfurization efficiency. DFT computational analysis on hypothetical supramolecular 1:1 complexes of the ILs with the three S-compounds examined shows that the interaction energies (ΔE kJ/mol) for **AIL1**⊃$DBTO_2$ are −105.10, − 86.71, − 84.75, and −82.74 kJ/mol in the gas phase, *n*-hexane, *n*-hexadecane, and CCl_4 solvent systems, respectively. On the other hand, the interaction energies (ΔE kJ/mol) for **AIL1**⊃DBT are −93.09, − 76.62, − 75.14, and −73.64 kJ/mol in the gas phase, *n*-hexane, *n*-hexadecane, and CCl_4 solvent systems, respectively. These results strongly suggest that the $\pi-\pi$ interactions and hydrogen bonds (O···H) in the complexes play essential roles in the interaction of the ionic liquids with DBT/$DBTO_2$. The DFT-calculated interaction energies support our experimental results.

https://doi.org/10.1021/acsomega.3c09975
ACS Omega 2024, 9, 23485−23498

■ ASSOCIATED CONTENT

Supporting Information

The Supporting Information is available free of charge at https://pubs.acs.org/doi/10.1021/acsomega.3c09975.

Spectra of **AL1** and **AL2** and their intermediates (PDF)

■ AUTHOR INFORMATION

Corresponding Authors

Shofiur Rahman − *Biological and Environmental Sensing Research Unit, King Abdullah Institute for Nanotechnology, King Saud University, Riyadh 11451, Saudi Arabia;* orcid.org/0000-0003-4219-4758; Email: mrahman1@ksu.edu.sa

Syed A. Imtiaz − *Department of Process Engineering, Memorial University of Newfoundland, St John's, Newfoundland and Labrador A1B3X5, Canada;* orcid.org/0000-0002-2715-9084; Email: simtiaz@mun.ca

Yan Zhang − *Department of Process Engineering, Memorial University of Newfoundland, St John's, Newfoundland and Labrador A1B3X5, Canada;* orcid.org/0000-0003-0107-1014; Email: yanz@mun.ca

Paris E. Georghiou − *Department of Chemistry, Memorial University of Newfoundland, St John's, Newfoundland and Labrador A1B3X5, Canada;* orcid.org/0000-0001-9435-6857; Email: parisg@mun.ca

Authors

Amani Sager − *Department of Process Engineering, Memorial University of Newfoundland, St John's, Newfoundland and Labrador A1B3X5, Canada*

Abdullah Alodhayb − *Biological and Environmental Sensing Research Unit, King Abdullah Institute for Nanotechnology, King Saud University, Riyadh 11451, Saudi Arabia;* orcid.org/0000-0003-0202-8712

Mahmoud Al-Gawati − *Biological and Environmental Sensing Research Unit, King Abdullah Institute for Nanotechnology, King Saud University, Riyadh 11451, Saudi Arabia*

Complete contact information is available at: https://pubs.acs.org/10.1021/acsomega.3c09975

Notes

The authors declare no competing financial interest.

■ ACKNOWLEDGMENTS

The authors extend their appreciation to the Deputyship for Research & Innovation, Ministry of Education in Saudi Arabia, for funding this research work through project no. (IFKSUOR3−303-4). The authors also thank Acenet and the Digital Research Alliance of Canada (alliancecan.ca) for the computing support.

■ REFERENCES

(1) Guo, J.; Li, Y.; Xiong, J.; Zhu, T. Coupling mechanism of activated carbon mixed with dust for flue gas desulfurization and denitrification. *J. Environ. Sci.* **2020**, *98*, 205−214.

(2) Zhao, Z.; Zhang, Y.; Gao, W.; Baleta, J.; Liu, C.; Li, W.; Weng, W.; Dai, H.; Zheng, C.; Gao, X. Simulation of SO_2 absorption and performance enhancement of wet flue gas desulfurization system. *Process Saf. Environ. Prot.* **2021**, *150*, 453−463.

(3) Li, X.; Han, J.; Liu, Y.; Dou, Z.; Zhang, T. Summary of research progress on industrial flue gas desulfurization technology. *Sep. Purif. Technol.* **2022**, *281*, No. 119849.

(4) Liu, P.; Yang, S.; Hu, J.; Wang, H. Numerical analysis of SO_2 removal characteristics in industrial flue gas desulfurization reactor by spray drying adsorption. *Sep. Purif. Technol.* **2023**, *323*, No. 124475.

(5) Huang, T.; Xu, J.; Fan, Y. Effects of concentration and microstructure of active phases on the selective hydrodesulfurization performance of sulfided CoMo/ Al_2O_3 catalysts. *Appl. Catal. B Environ.* **2018**, *220*, 42−56.

(6) Al-Jamimi, H. A.; Saleh, T. A. Transparent predictive modelling of catalytic hydrodesulfurization using an interval type-2 fuzzy logic. *J. Clean. Prod.* **2019**, *231*, 1079−1088.

(7) Ali, I.; Al-Arfaj, A. A.; Saleh, T. A. Carbon nanofiber-doped zeolite as support for molybdenum based catalysts for enhanced hydrodesulfurization of dibenzothiophene. *J. Mol. Liq.* **2020**, *304*, No. 112376.

(8) Saleh, T. A. Carbon nanotube-incorporated alumina as a support for MoNi catalysts for the efficient hydrodesulfurization of thiophenes. *Chem. Eng. J.* **2021**, *404*, No. 126987.

(9) Ali, I.; Saleh, T. A. Zeolite-graphene composite as support for molybdenum-based catalysts and their hydrodesulfurization performance. *Appl. Catal. A Gen.* **2020**, *598*, No. 117542.

(10) Ho, T. C. Deep HDS of diesel fuel: chemistry and catalysis. *Catal. Today* **2004**, *98*, 3−18.

(11) Menzel, R.; Iruretagoyena, D.; Wang, Y.; Bawaked, S. M.; Mokhtar, M.; Al-Thabaiti, S. A.; Basahel, S. N.; Shaffer, M. S. Graphene oxide/mixed metal oxide hybrid materials for enhanced adsorption desulfurization of liquid hydrocarbon fuels. *Fuel* **2016**, *181*, 531−536.

(12) Saleh, T. A.; Sulaiman, K. O.; Al-Hammadi, S. A.; Dafalla, H.; Danmaliki, G. I. Adsorptive desulfurization of thiophene, benzothiophene and dibenzothiophene over activated carbon manganese oxide nanocomposite: with column system evaluation. *J. Clean Prod.* **2017**, *154*, 401−412.

(13) Wang, J.; Zhang, Q.; Yang, H.; Qiao, C. Adsorptive desulfurization of organic sulfur from model fuels by active carbon supported Mn (II): equilibrium, kinetics, and thermodynamics. *Int. J. Chem. Eng.* **2020**, *2022*, 12.

(14) Huo, Q.; Li, J.; Liu, G.; Qi, X.; Zhang, X.; Ning, Y.; Zhang, B.; Fu, Y.; Liu, S. Adsorption desulfurization performances of Zn/Co porous carbons derived from bimetal-organic frameworks. *Chem. Eng. J.* **2019**, *362*, 287−297.

(15) Jafarinasab, M.; Akbari, A.; Omidkhah, M.; Shakeri, M. An efficient co-based metal-organic framework nanocrystal (Co-ZIF-67) for adsorptive desulfurization of dibenzothiophene: impact of the preparation approach on structure tuning. *Energy Fuels* **2020**, *34*, 12779−12791.

(16) Ganiyu, S. A.; Lateef, S. A. Review of adsorptive desulfurization process: Overview of the non-carbonaceous materials, mechanism and synthesis strategies. *Fuel* **2021**, *294*, No. 120273.

(17) Saha, B.; Vedachalam, S.; Dalai, A. K. Review on recent advances in adsorptive desulfurization. *Fuel Process. Technol.* **2021**, *214*, No. 106685.

(18) Hernández-Maldonado, A. J.; Yang, R. T. Desulfurization of Commercial Liquid Fuels by Selective Adsorption via π-Complexation with Cu(I)−Y Zeolite. *Ind. Eng. Chem. Res.* **2023**, *42*, 3103−3110.

(19) Chandran, D.; Khalid, M.; Walvekar, R.; Mubarak, N. M.; Dharaskar, S.; Wong, W. Y.; Gupta, T. C. S. M. Deep eutectic solvents for extraction-desulphurization: a review. *J. Mol. Liq.* **2019**, *275*, 312−322.

(20) Jha, D.; Haider, M. B.; Kumar, R.; Balathanigaimani, M. S. Extractive desulfurization of fuels using diglycol based deep eutectic solvents. *J. Environ. Chem. Eng.* **2020**, *8*, No. 104182.

(21) Wang, R. Z. A.; Qin, H.; Wang, J. W.; Cheng, H. Y.; Chen, L. F.; Qi, Z. W. Reactive extraction for intensifying 2-ethylhexyl acrylate synthesis using deep eutectic solvent Im:2PTSA. *Green Energy Environ.* **2021**, *6* (3), 405−412.

(22) Xu, L. X.; Luo, Y. P.; Liu, H.; Yin, J.; Li, H. P.; Jiang, W.; Zhu, W. S.; Li, H. M.; Ji, H. B. Extractive desulfurization of diesel fuel by amide-based type IV deep eutectic solvents. *J. Mol. Liq.* **2021**, *338*, No. 116620.

(23) Jiang, W.; Zhu, K.; Jia, H.; Zhu, L.; Wang, C.; Xu, L.; Li, H.; Zhu, W.; Li, H. Synthesis of task-specific ternary deep eutectic solvents for deep desulfurization via reactive extraction. *Chem. Eng. Process.* **2022**, *171*, No. 108754.
(24) Ahmad, A.; Zamzami, M. A.; Ahmad, V.; Al-Thawadi, S.; Akhtar, M. S.; Khan, M. J. Bacterial biological factories intended for the desulfurization of petroleum products in refineries. *Fermentation* **2023**, *9*, 211.
(25) Kodama, K.; Umehara, K.; Shimizu, K.; Nakatani, S.; Minoda, Y.; Yamada, K. Identification of microbial products from dibenzothiophene and its proposed oxidation pathway. *Agric. Biol. Chem.* **1973**, *37*, 45−50.
(26) Dehkordi, A. M.; Sobati, M. A.; Nazem, M. A. Oxidative desulfurization of non-hydrotreated kerosene using hydrogen peroxide and acetic acid. *Chin. J. Chem. Eng.* **2009**, *17*, 869−874.
(27) Yu, G.; Lu, S.; Chen, H.; Zhu, Z. Oxidative desulfurization of diesel fuels with hydrogen peroxide in the presence of activated carbon and formic acid. *Energy Fuels* **2005**, *19*, 447−452.
(28) Mirshafiee, F.; Movahedirad, S.; Sobati, M. A.; Alaee, R.; Zarei, S.; Sargazi, H. Current status and future prospects of oxidative desulfurization of naphtha: a review. *Process Safety and Environ. Protect.* **2023**, *170*, 54−75.
(29) Rakhmanov, E. V.; Domashkin, A. A.; Myltykbaeva, Z. K.; Kairbekov, Z.; Shigapova, A. A.; Akopyan, A. V.; Anisimov, A. V. Peroxide oxidative desulfurization of a mixture of nonhydrotreated vacuum gas oil and diesel fraction. *Petrol. Chem.* **2016**, *56*, 742−744.
(30) Hossain, M. N.; Park, H. C.; Choi, H. S. A comprehensive review on catalytic oxidative desulfurization of liquid fuel oil. *Catalysts.* **2019**, *9*, 229.
(31) Akopyana, A. V.; Esevaa, E. A.; Polikarpovaa, P. D.; Kedaloa, A. A.; Anisimova, A. V. Oxidation of condensed thiophene derivatives with Brønsted acidic ionic liquid. *Moscow Univ. Chem. Bull.* **2019**, *74*, 284−289.
(32) Akopyan, A.; Eseva, E.; Polikarpova, P.; Kedalo, A.; Vutolkina, A.; Glotov, A. Deep oxidative desulfurization of fuels in the presence of Brönsted acidic polyoxometalate-based ionic liquids. *Molecules* **2020**, *25*, 536.
(33) Lo, W. H.; Yang, H. Y.; Wei, G. T. One-pot desulfurization of light oils by chemical oxidation and solvent extraction with room temperature ionic liquids. *Green Chem.* **2003**, *5*, 639−642.
(34) Hao, D.; Hao, L.; Deng, C.; Ren, W.; Guo, C.; Lü, H. Removal of dibenzothiophene from diesels by extraction and catalytic oxidation with acetamide-based deep eutectic solvents. *Chem. Eng. Technol.* **2019**, *42*, 1276−1282.
(35) Saini, N.; Yadav, P.; Kumar, K.; Ghosh, P. Oxidative extractive desulfurization of fuel catalyzed via carboxylic acid and metal halides. *Materials Today: Proceedings* **2023**, *73*, 189−194.
(36) Pandey, S.; Srivastava, V. C. Oxidative-extractive desulfurization of liquid fuel using stannous chloride-acetic acid mixture as catalyst. *Petrol. Sci. Technol.* **2018**, *36*, 40−47.
(37) Dhameliya, T. M.; Nagar, P. R.; Bhakhar, K. A.; Jivani, H. R.; Shah, B. J.; Patel, K. M.; Patel, V. S.; Soni, A. H.; Joshi, L. P.; Gajjar, N. D. Recent advancements in applications of ionic liquids in synthetic construction of heterocyclic scaffolds: A spotlight. *J. Mol. Liq.* **2022**, *348*, No. 118329.
(38) Hallett, J. P.; Welton, T. Room-temperature ionic liquids: Solvents for synthesis and catalysis. 2. *Chem. Rev.* **2011**, *111*, 3508−3576.
(39) Badgujar, K. C.; Badgujar, V. C.; Bhanage, B. M. Recent update on use of ionic liquids for enzyme immobilization, activation, and catalysis: A partnership for sustainability. *Curr. Opinion Green Sustain. Chem.* **2022**, *36*, No. 100621.
(40) Karuppasamy, K.; Theerthagiri, J.; Vikraman, D.; Yim, C. J.; Hussain, S.; Sharma, R.; Maiyalagan, T.; Qin, J.; Kim, H. S. Ionic liquid-based electrolytes for energy storage devices: A brief review on their limits and applications. *Polymers* **2020**, *12*, 918.
(41) Tang, X.; Lv, D.; Jiang, K.; Zhou, G.; Liu, X. Recent development of ionic liquid-based electrolytes in lithium-ion batteries. *J. Power Sources.* **2022**, *542*, No. 231792.
(42) Nikfarjam, N.; Ghomi, M.; Agarwal, T.; Hassanpour, M.; Sharifi, E.; Khorsandi, D.; Ali Khan, M.; Rossi, F.; Rossetti, A.; Nazarzadeh, Z. E.; Rabiee, N.; Afshar, D.; Vosough, M.; Maiti, T. K.; Mattoli, V.; Lichtfouse, E.; Tay, F. R.; Makvandi, P. Antimicrobial ionic liquid-based materials for biomedical applications. *Adv. Funct. Mater.* **2021**, *42*, No. 2104148.
(43) Zhang, Y.; Liu, C.; Wang, J.; Ren, S.; Song, Y.; Quan, P.; Fang, L. Ionic liquids in transdermal drug delivery system: Current applications and future perspectives. *Chin. Chem. Lett.* **2023**, *34*, No. 107631.
(44) Greer, A. J.; Jacquemin, J.; Hardacre, C. Industrial Applications of Ionic Liquids. *Molecules* **2020**, *25*, 5207.
(45) Hosseini, A.; Khoshsima, A.; Sabzi, M.; Rostam, A. Toward application of ionic liquids to desulfurization of fuels: A review. *Energy Fuels* **2022**, *36*, 4119−4152.
(46) Desai, K.; Dharaskar, S.; Khalid, M.; Gedam, V. Effectiveness of ionic liquids in extractive−oxidative desulfurization of liquid fuels: a review. *Chem. Pap.* **2022**, *76*, 1989−2028.
(47) Singh, S. K.; Savoy, A. W. Ionic liquids synthesis and applications: An overview. *J. Mol. Liq.* **2020**, *297*, No. 112038.
(48) Jha, D.; Maheshwari, P.; Singh, Y.; Haider, M. B.; Kumar, R.; Balathanigaimani, M. S. A comparative review of extractive desulfurization using designer solvents: Ionic liquids & deep eutectic solvents. *J. Ener. Inst.* **2023**, *110*, No. 101313.
(49) Hayes, R.; Warr, G. G.; Atkin, R. Structure and nanostructure in ionic liquids. *Chem. Rev.* **2015**, *115*, 6357−6426.
(50) (a) Mohumed, H.; Rahman, S.; Imtiaz, S. A.; Zhang, Y. Oxidative-extractive desulfurization of model fuels using a pyridinium ionic liquid. *ACS omega* **2020**, *5* (14), 8023−8031. (b) Zhao, H.; Baker, G. A.; Wagle, D. V.; Ravula, S.; Zhang, Q. Tuning task-specific ionic liquids for the extractive desulfurization of liquid fuel. *ACS Sustain. Chem. Eng.* **2016**, *4*, 4771−4780.
(51) Zhao, H.; Baker, G. A.; Wagle, D. V.; Ravula, S.; Zhang, Q. Tuning task-specific ionic liquids for the extractive desulfurization of liquid fuel. *ACS Sustain. Chem. Eng.* **2016**, *4*, 4771−4780.
(52) Wilfred, C. D.; Kiat, C. F.; Man, Z.; Bustam, M. A.; Mutalib, M. I. M.; Phak, C. Z. Extraction of dibenzothiophene from dodecane using ionic liquids. *Fuel Proc. Technol.* **2012**, *93*, 85−89.
(53) Zhang, C.; Pan, X.; Wang, F.; Liu, X. Extraction−oxidation desulfurization by pyridinium-based task-specific ionic liquids. *Fuel* **2012**, *102*, 580−584.
(54) Jiang, W.; Zhu, K.; Li, H.; Zhu, L.; Hua, M.; Xiao, J.; Wang, C.; Yang, Z.; Chen, G.; Zhu, W. Synergistic effect of dual Brønsted acidic deep eutectic solvents for oxidative desulfurization of diesel fuel. *Chem. Eng. J.* **2020**, *394*, No. 124831.
(55) Dong, Y.; Nie, Y.; Zhou, Q. Highly efficient oxidative desulfurization of fuels by Lewis acidic ionic liquids based on iron chloride. *Chem. Eng. Technol.* **2013**, *36*, 435−442.
(56) Nie, Y.; Dong, Y.; Bai, L.; Dong, H.; Zhang, X. Fast oxidative desulfurization of fuel oil using dialkylpyridinium tetrachloroferrates ionic liquids. *Fuel* **2013**, *103*, 997−1002.
(57) Andevary, H. H.; Akbari, A.; Omidkhah, M. High efficient and selective oxidative desulfurization of diesel fuel using dual-function [Omim]$FeCl_4$ as catalyst/extractant. *Fuel Process. Technol.* **2019**, *185*, 8−17.
(58) Wang, X.; Han, M.; Wan, H.; Yang, C.; Guan, G. Study on extraction of thiophene from model gasoline with Brönsted acidic ionic liquids. *Front. Chem. Sci. Eng.* **2011**, *5*, 107−112.
(59) Chen, X.; Guan, Y.; Abdeltawab, A. A.; Al-Deyab, S. S.; Yuan, X.; Wang, C.; Yu, G. Using functional acidic ionic liquids as both extractant and catalyst in oxidative desulfurization of diesel Fuel: An investigation of real feedstock. *Fuel* **2015**, *146*, 6−12.
(60) Liu, D.; Gui, J.; Park, Y. K.; Yang, S.; Gao, Y.; Peng, X.; Sun, Z. Deep removal of sulfur from real diesel by catalytic oxidation with halogen-free ionic liquid. *Korean J. Chem. Eng.* **2012**, *29*, 49−53.
(61) Zhang, C.; Pan, X.; Wang, F.; Liu, X. Extraction−oxidation desulfurization by pyridinium-based task-specific ionic liquids. *Fuel* **2012**, *102*, 580−584.

https://doi.org/10.1021/acsomega.3c09975
ACS Omega 2024, 9, 23485−23498

(62) Rahman, S.; Georghiou, P. E.; Alodhayb, A.Density functional theory (DFT) models for the desulfurization and extraction of sulfur compounds from fuel oils using ionic liquids, in *Modeling of Chemical Process Systems*, Ed. Imtiaz, S. A.Elsevier: Amsterdam, 2023.
(63) Frisch, M. J.; Trucks, G. W.; Schlegel, H. B.; Scuseria, G. E.; Robb, M. A.; Cheeseman, J. R.; Scalmani, G.; Barone, V. V.; Petersson, G. A. G. A.; Nakatsuji, H.et al.*Gaussian 16, Revision C.01*; Gaussian, Inc.: Wallingford, 2019.
(64) Dennington, R.; Keith, T. A.; Millam, J.*GaussView*, Version 6.0.16, Semichem Inc.: Shawnee Mission, KS USA, 2019.
(65) Otsuki, S.; Nonaka, T.; Takashima, N.; Qian, W.; Ishihara, A.; Imai, T.; Kabe, T. Oxidative desulfurization of light gas oil and vacuum gas oil by oxidation and solvent extraction. *Energy Fuel.* **2000**, *14*, 1232−1239.
(66) Fukui, K.; Yonezawa, T.; Shingu, H. A molecular orbital theory of reactivity in aromatic hydrocarbons. *J. Chem. Phys.* **1952**, *20*, 722−725.
(67) Luo, J.; Xue, Z. Q.; Liu, W. M.; Wu, J. L.; Yang, Z. Q. Koopmans' theorem for large molecular systems within density functional theory. *J. Phys. Chem. A* **2006**, *110*, 12005−12009.
(68) Hizaddin, F. H.; Anantharaj, R.; Hashim, M. A. 2014. A quantum chemical study on the molecular interaction between pyrrole and ionic liquids. *J. Mol. Liq.* **2014**, *194*, 20−29.
(69) Gu, P.; Lu, R.; Liu, D.; Lu, Y.; Wang, S. Exploring the nature of interactions among thiophene, thiophene sulfone, dibenzothiophene, dibenzothiophene sulfone and a pyridinium-based ionic liquid. *Phys. Chem. Chem. Phys.* **2014**, *16*, 10531−10538.
(70) Murray, J. S.; Politzer, P. The electrostatic potential: an overview. *Wiley Interdiscip. Rev.: Comput. Mol. Sci.* **2011**, *2011* (1), 153−163.
(71) Murray, J. S.; Sen, K. in *Molecular Electrostatic Potentials, Concepts and Applications*; Elsevier: Amsterdam, 1996.
(72) Politzer, P.; Murray, J. The fundamental nature and role of the electrostatic potential in atoms and molecules. *Theor. Chem. Acc.* **2002**, *108*, 134−142.

https://doi.org/10.1021/acsomega.3c09975
ACS Omega 2024, 9, 23485−23498